Electronic Structure of ABC-stacked Multilayer Graphene and Trigonal Warping:A First Principles Calculation

Electronic Structure of ABC-stacked Multilayer Graphene and Trigonal Warping:A First Principles Calculation

Celal Yelgel

Recep Tayyip Erdogan University, Faculty of Engineering, Department of Materials Science and Nanotechnology Engineering, 53100, Rize, Turkey

E-mail: celal.yelgel@erdogan.edu.tr

Abstract. We present an extensive density functional theory (DFT) based investigation of the electronic structures of ABC–stacked N–layer graphene. It is found that for such systems the dispersion relations of the highest valence and the lowest conduction bands near the **K** point in the Brillouin zone are characterised by a mixture of cubic, parabolic, and linear behaviours. When the number of graphene layers is increased to more than three, the separation between the valence and conduction bands decreases up until they touch each other. For five and six layer samples these bands show flat behaviour close to the **K** point. We note that all states in the vicinity of the Fermi energy are surface states originated from the top and/or bottom surface of all the systems considered. For the trilayer system, N=3, pronounced trigonal warping of the bands slightly above the Fermi level is directly obtained from DFT calculations.

1. Introduction

Graphene has become one of the most investigated systems due to its remarkable electronic, mechanical and thermal properties [1, 2]. Experiments reveal that the single layer graphene and stacks of graphene layers can be used in the design of new electronic devices [3, 4, 5]. In addition to the fascinating development in research on properties of graphene and bilayer graphene, few-layer graphene (FLG) has also gained recent attention [6, 7, 8, 9]. The ability of creating stacks of the individual graphene sheets in FLG provides an extra degree of freedom on electronic properties [10, 11, 12, 13]. It has been predicted and suggested that different stacking orders, with distinct lattice symmetries, have a forceful effect on the band structure and electronic properties of FLG [14, 15]. Experimentally, the strong influence of stacking order on the low–energy electronic structure of FLG was recently demonstrated by infrared (IR) spectroscopy [10]. The band structures of graphene from one to four layers were also measured using angle–resolved photoemission spectroscopy [16].

Although the FLG and graphite are mostly Bernal–stacked (AB), trilayer graphene has two different stacking orders: ABA (Bernal) and ABC (rhombohedral). These stackings for trilayer graphene are expected to be metal–like [17] and predicted as two stable configurations in Refs. [9, 11, 18]. Even though there are small cohesive energy differences between these two types of trilayer graphene, recent studies indicate that they exhibit very different electronic properties [11, 12, 19]. A recent study of the electronic structure of the ABA– and ABC–stacked multilayer graphene was reported by using tight–binding approach and density functional theory

[11, 20, 21, 22, 23]. The work in Ref. [22] shows that the type of interlayer coupling present in ABC–stacked multilayer with N layers graphene gives rise to trigonal warping of the energy bands near the Fermi surface that is both qualitatively and quantitatively different from that in bilayer graphene.

In the present work, we investigate the band structure of ABC–stacked N–layer graphene by employing the plane wave pseudopotential method within the density functional scheme. The orbital natures of the highest occupied molecular orbital (HOMO) and lowest unoccupied molecular orbital (LUMO) states are investigated using partial charge density plots. We note that these states are characterised as surface states which form flat bands around the Fermi level, with an increasing the **k** space near the **K** point with the number of layers N. Our calculations indicate that the dispersion curve of the highest valence and lowest conduction bands for the ABC–stacked N-layer graphene are a mixture of cubic, quadratic, and linear behaviours. The nature of the trigonal warping of energy bands slightly above the Fermi level is examined for different layer thicknesses. This is achieved through an examination of the orbital origins of the highest occupied and lowest unoccupied bands at the Dirac (**K**) point. The trigonal warping effect of the energy bands near the Fermi level is also discussed using the constant electron energy countour plots.

2. Computational Method

Our total-energy and electronic-structure calculations were performed in the framework of the first-principles plane wave pseudopotential method within the local density approximation of the density functional theory (LDA-DFT). The ABC–stacked trilayer and multilayer graphene were modelled by using a repeated slab geometry. To avoid interaction between neighbouring slabs along the normal direction, a 15 Å vacuum region was used to separate them after several converge tests. The interlayer separation was found to be 3.33 Å with our theoretical lattice constant of 2.46 Å. The Perdew-Zunger exchange correlation scheme [24] was employed for electron-electron interaction. Norm-conserving [25] and fully separable [26] pseudopotentials for C were used to treat electron-ion interaction. Single-particle Kohn-Sham orbitals were expanded by using a plane-wave basis set with a kinetic energy cutoff of 40 Ryd. Self-consistent solutions of the Kohn-Sham equations were obtained by employing a $36 \times 36 \times 2$ **k**-points Monkhorst-Pack set [27] within the supercell Brillouin zone. Relaxed atomic positions were obtained by using the total energy and force minimisation methods. Details of the theoretical method employed in our work can be found in Refs. [28, 29].

3. Results

Before presenting results, we briefly discuss the appropriateness of the LDA-DFT method employed in our investigation. It has widely been mentioned that electron-electron interactions in graphene and graphite should be described by a combination of van der Waals (vdW) and density functional schemes. Indeed, there are some recent proposals to calculate vdW interactions within the DFT approach [30, 31, 32, 33, 34]. However, systematic improvement of results from the vdW-DFT theory has not yet been evidenced for all systems. For example, agreement between theory and experiment for interlayer spacing in graphite is less favourable from the vdW-DFT theory than from the LDA-DFT theory [35]. It has been concluded that for systems that LDA finds to be weakly bonded, the binding energies obtained with the vdW-DFT and LDA-DFT methods are very similar [36]. We thus expect that the LDA-DFT scheme will produce reasonably acceptable results for our system of the ABC–stacked N–layer graphene.

We first start with the ABC–stacked trilayer graphene (the $N = 3$ trilayer case). There are six basis carbon atoms in its unit cell, with two basis carbon atoms in each layer. As illustrated in Fig. 1, while the bottom and middle layers of the ABC-stacked trilayer graphene are arranged in Bernal (AB), the basis C_{31} in the top layer lies exactly above the basis C_{22} in the middle

layer and the second basis C_{32} on the top layer is at the centre of the hexagon formed by the carbon atoms in the bottom layer. The interlayer separation is found to be 3.33 Å by using our theoretical lattice constant of 2.46 Å after several total energy calculations. This result is in good agreement with experimentally measured interlayer distance of graphite [37].

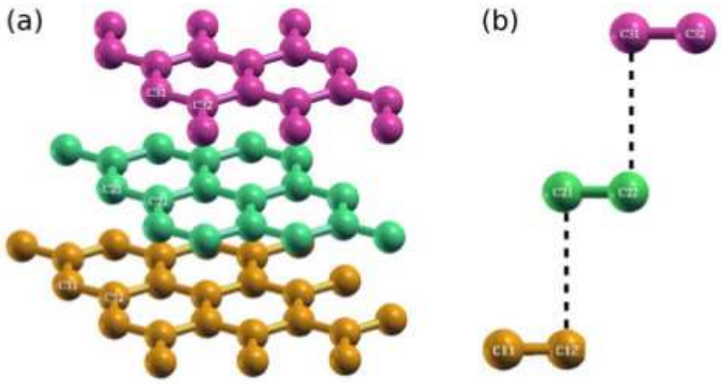

Figure 1. (a) Atomic structure of ABC–stacked trilayer graphene containing six basis carbon atoms in the primitive unit cell. (b) Schematic of the unit cell of ABC–stacked trilayer graphene.

The electronic band structure was examined close to the Dirac point (the **K** point in the Brillouin zone) for wavevectors lying in graphene plane. As represented in Fig. 2, along k_x two bands lying close to the Fermi energy cross each other, thus indicating metallic behaviour of the system. These bands, however, do not cross each other for $-k_x$ values, indicating semiconducting

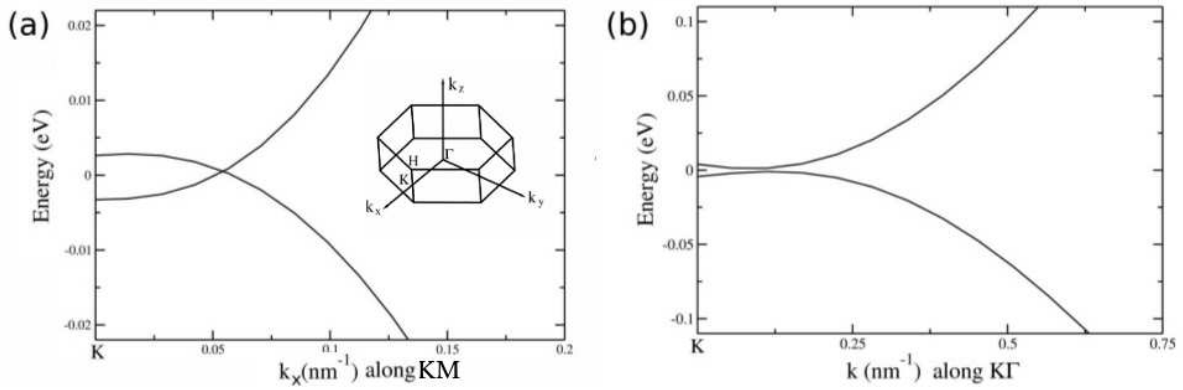

Figure 2. Band structure of the ABC–stacked trilayer graphene close to **K** point (a) along k_x (the **KM** direction), (b) along $-k_x$ (the **K**Γ direction). The Fermi level is set to zero energy. The hexagonal Brillouin zone is also shown as an inset.

behaviour along the $\mathbf{K}-\mathbf{\Gamma}$ direction. A similar behaviour of these bands are also found in the work of Latil and Henrard [11]. A polynomial fit of the part of the curve in Fig. 3 (a) shows a mixture of linear, quadratic and cubic terms:

$$E = a_0 + a_1 k_x + a_2 k_x^2 + a_3 k_x^3, \tag{1}$$

where k_x is expressed in nm^{-1}, E in eV, and a_0=-0.004 eV, a_1=0.0027 eV nm, a_2=0.91 eV nm^2, a_3=4.524 eV nm^2.

We calculated the constant energy contours using a 50×50 mesh around the **K** point, which results in consideration of 2500 **k**-points. For the ABC–stacked trilayer graphene energy contour plots up to the energy values 0.85 eV above and 0.72 eV below the Fermi level and close to the **K** point are shown in Fig. 3 (b) and (c). In the Fig. 3 (b), the lowest energy contours appear to be located at 0.26 nm^{-1} from the **K** point and 45 meV above the Fermi level. These energy contour plots clearly indicate prominent trigonal warping – stretching of equienergy lines along directions at 120° from each other.

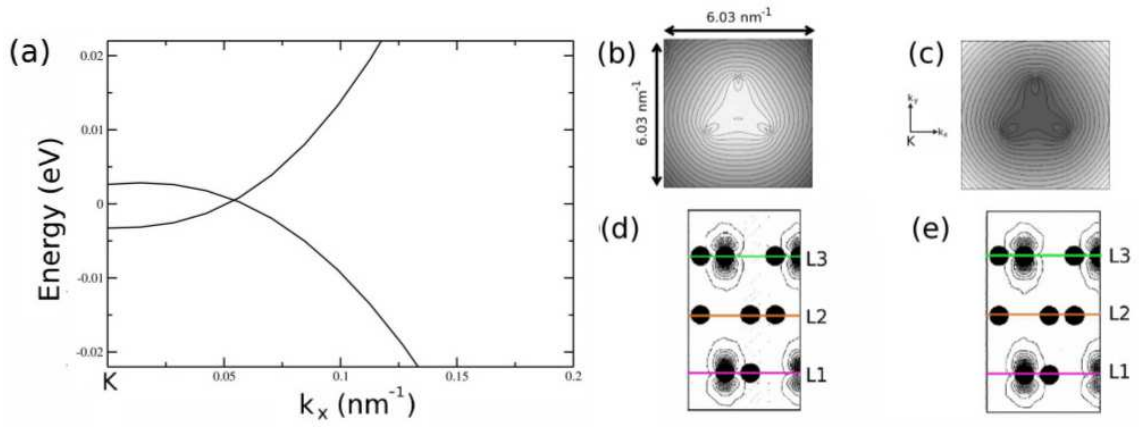

Figure 3. (a) Band structure of ABC–stacked $N = 3$ layer graphene close to **K** point with the energy zero set at the Fermi level. The electronic energy contour plots for (b) the lowest conduction band up to 0.85 eV above the Fermi level and (c) the highest valence up to 0.72 eV below the Fermi level. The minumum and maximum energies in the contour plots are shown as the lighest and darkest colours, respectively. Electronic charge density contour plots at the **K** point are also given for (d) the lowest conduction band and (e) the highest valance band.

We now model ABC–stacked multilayer graphene. In particular, we consider the N–layer stacking sequences ABCA, ABCAB, and ABCABC with $N = 4$, $N = 5$ and $N = 6$, respectively. For the $N = 4$ multilayer the top layer graphene sheet is exactly above the bottom layer of the ABC–stacked trilayer. In general, for $N > 3$ the top layer graphene sheet lies exactly above the $(N - 3)^{\text{rd}}$ layer(s).

The innermost pair of bands for $N = 4$ are shown in Fig. 4 (a). The two bands are degenerate at the **K** point at which the Fermi level lies. These bands split by a maximum of 2.5 meV slightly away from **K** along k_x and then cross each other at a slightly larger value of the wavevector. This result is also in good agreement with the work in Ref. [11]. The pronounced trigonal warping seen for $N = 3$ system has been reduced for the $N = 4$ case. Figure 4 (b) and (c) show the energy contour plots up to 0.80 eV above and 0.65 eV below the Fermi level.

As shown in Fig. 5 (a), when the graphene thickness is increased to $N = 5$ layers, the innermost pair of bands become quite flat around the Fermi level very close to the **K** point. With the increase in the wavevector along k_x, these bands cross each other twice in the close vicinity of the **K** point. Between the two crossings there is a maximum splitting of approximately 10 meV between these bands. The amount of this splitting is larger than that for the $N = 3$ and $N = 4$ cases. The energy contour plots in 5 (b) and (c) reveal that the trigonal warping present for N=3 is almost lost for the N=5 system.

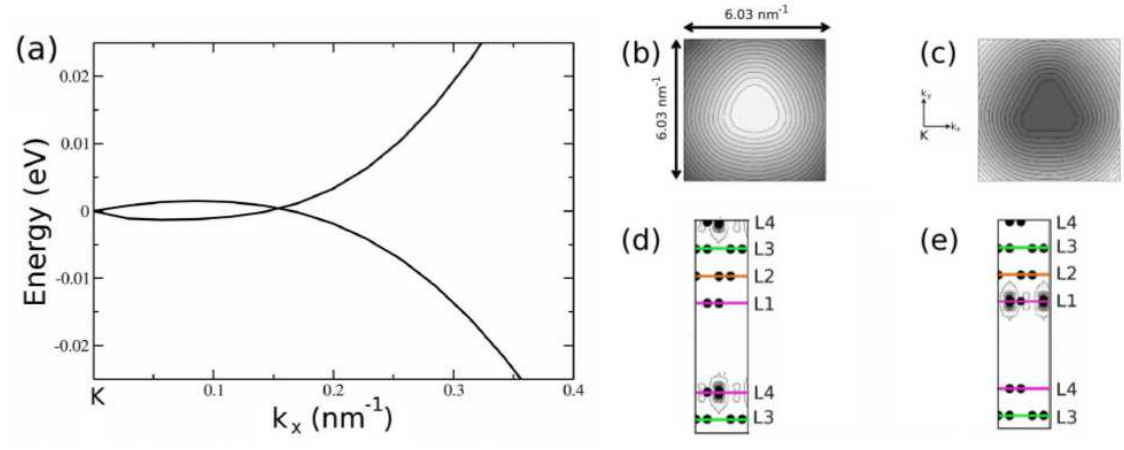

Figure 4. (a) Band structure of ABC–stacked $N = 4$ layer graphene close to **K** point with the energy zero set at the Fermi level. Energy contour plots for (b) low conduction bands up to 0.80 eV above the Fermi level, and (c) high valence bands up to 0.65 eV below the Fermi level. The minumum and maximum energies in the contour plots are shown as the lighest and darkest colours, respectively. Partial charge density plots at the **K** point also given for (d) the lowest conduction band and (e) the highest valence band.

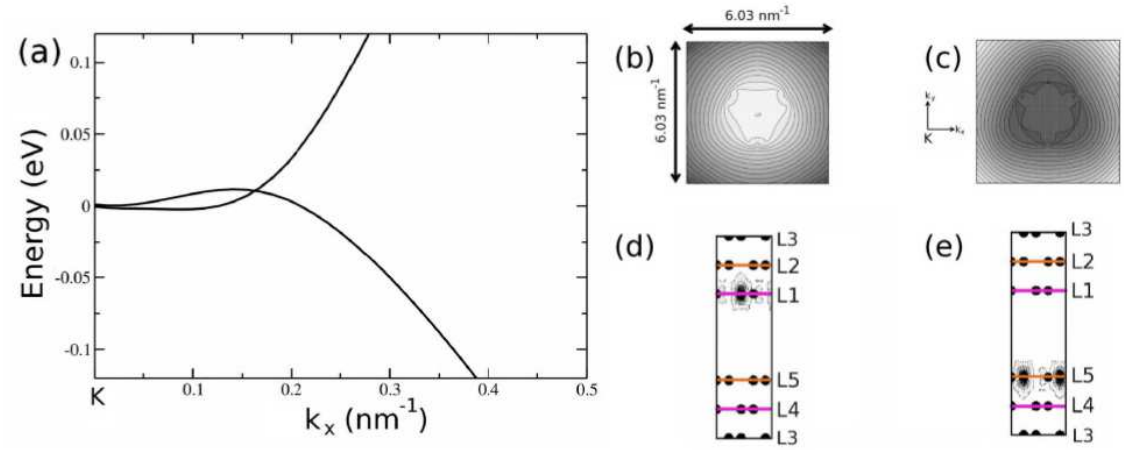

Figure 5. (a) Band structure of ABC–stacked $N = 5$ layer graphene close to **K** point with the energy zero set at the Fermi level. Energy contour plots for (b) low conduction bands up to 0.86 eV above the Fermi level and (c) high valence bands up to 0.61 eV below the Fermi level. The minumum and maximum energies in the contour plots are shown as the lighest and darkest colours, respectively. Partial charge density plots at the **K** point are also given for (d) the lowest conduction band and (e) the highest valence band.

The electronic band structure of the ABC–stacked 6–layer graphene is presented in Fig. 6 (a). There is a small amount of separation between the two bands around the Fermi level at the **K** point. These bands become degenerate slightly away from **K** point and remain so for some distance along k_x, in contrast with the $N = 3, 4, 5$ cases. The trigonal warping is found to be

quite weak for this system, as seen in Fig. 6 (b) and (c).

In order to examine the origin of the HOMO and LUMO energy states at the **K** point, we made partial charge density plots in a vertical plane for ABC–stacked N–layer graphene. It is found that for N=3 and N=6 both HOMO and LUMO states are derived from the appropriate combinations of the p_z orbitals on the first basis atom (C_{11}) on the bottommost layer and the second basis atom (C_{32} or C_{62}) on the topmost layer. In contrast, for N=4 and N=5, both HOMO and LUMO have maximum contribution from the p_z orbital of only one basis atom, either on the bottommost or the uppermost layer. The largest contribution for HOMO comes from C_{11} for N=4 and from C_{52} for N=5. The largest contribution for LUMO comes from C_{42} for N=4 and from C_{11} for N=5. These features can be seen in the contour plots presented in the Figs. 3-6 (d) and (e).

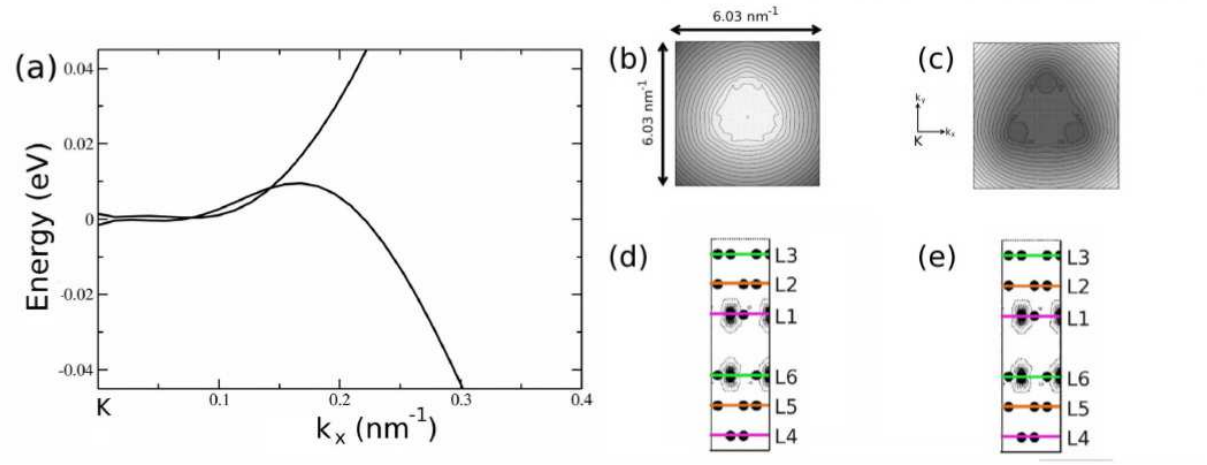

Figure 6. (a) Band structure of ABC–stacked N = 6 layer graphene close to **K** point with the energy zero set at the Fermi level. Energy contour plots for (b) low conduction bands up to 0.83 eV above the Fermi level and (c) high valence bands up to 0.61 eV below the Fermi level. The minumum and maximum energies in the contour plots are shown as the lighest and darkest colours, respectively. Partial charge density plots at the **K** point are also given for (d) the lowest conduction band and (e) the highest valence band.

We have noted that the HOMO and LUMO states for the ABC–stacked N–layer graphene systems studied here are surface states which form flat bands around the Fermi level. In fact any size of few–layer graphene system, thicker than the bi–layer graphene, can be viewed as a thin slab. Our analysis clearly suggests that the HOMO and LUMO states of the ABC–stacked N–layer graphene systems originate from the top and/or bottom surface of the slab. The surface feature extracted in our work has gone un-noticed in previous investigations of such systems.

4. Summary

In summary, we have studied the ABC–stacked N–layer graphene by using the density functional theory within the local approximation and the plane wave pseudopotential method. The dispersion of π/π^* bands close to Dirac point is established to show a mixture of cubic, quadratic, and linear behaviours for the ABC–stacked trilayer graphene. Equienergy contour plots clearly indicate prominent trigonal warping in the ABC–stacked system– stretching of equienergy lines along directions at 120° from each other. ABC–stacked systems with layer numbers $N > 3$ are characterised with much reduced level of trigonal warping. Our first-principles results for the

warping of equienergy contours have good agreement with the tight-binding results [22]. From an analysis of partial charge density plots, we have established that the highest occupied state and the lowest unoccupied state at the **K** point originate from the p_z orbitals of carbon atoms in the bottom and uppermost layers of the N=3 and N=6 systems, but only from one of the layers for the N=4 and N=5 systems. Thus the HOMO and LUMO states of the N–layer graphene systems can be regarded as surface states.

References

[1] Novoselov K S, Geim A K, Morozov S V, Jiang D, Zhang Y, Dubonos S V, Gregorieva I V and Firsov A A 2004 *Science* **306** 666
[2] Zhang Y, Small J P, Amori S and Kim P 2005 *Phys. Rev. Lett.* **94** 176803
[3] Berger C, Song Z M, Li T B, Li X, Ogbazghi A Y, Feng R, Dai Z, Marchenkov A N, Conrad E H, First P N and De Heer W A 2004 *J. Phys. Chem.* B **108** 19912
[4] Bunch J S, Yaish Y, Brink M, Bolotin K and McEuen P L 2005 *Nano Lett.* **5** 2887
[5] Novoselov K S, Jiang D, Schedin F, Booth T J, Khotkevich V V, Morozov S V and Geim A K 2005 *Proc. Natl. Acad. Sci.* **102** 10451
[6] Zhu W J, Perebeinos V, Freitag M and Avouris P 2009 *Phys. Rev.* B **80** 235402
[7] Bao W Z, Zhao Z, Zhang H, Liu G, Kratz P, Jing L, Velasco J, Smirnov D and Lau C N 2010 *Phys. Rev. Lett.* **105** 246601
[8] Ghosh S, Bao W Z, Nika D L, Subrina S, Pokatilov E P, Lau C N and Balandin A A 2010 *Nat. Mater.* **9** 555
[9] Guinea F, Castro Neto A H and Peres N M R 2006 *Phys. Rev.* B **73** 245426
[10] Mak K F, Shan J and Heinz T F 2010 *Phys. Rev. Lett.* **104** 176404
[11] Latil S and Henrard L 2006 *Phys. Rev. Lett.* **97** 036803
[12] Aoki M and Amawashi H 2007 *Solid State Comm.* **142** 123
[13] Norimatsu W and Kusunoki M 2010 *Phys. Rev.* B **81** 161410
[14] Avetisyan A A, Partoens B and Peeters F M 2008 *Phys. Rev. B* **80** 195401
[15] McCann E and Koshino M 2010 *Phys. Rev.* B **81** 241409
[16] Ohta T, Bostwick A, Seyller T, Horn K and Rotenberg E 2006 *Science* **313** 951
[17] Yuan S, De Raedt H and Katsnelson M I 2010 *Phys. Rev.* B **82** 235409
[18] Guinea F, Castro A H and Peres N M R 2007 *Solid State Comm.* **143** 116
[19] Nakamura M and Hirasawa L 2008 *Phys. Rev.* B **77** 045429
[20] Koshino M and McCann E 2009 *Phys. Rev.* B **79** 125443
[21] Koshino M and Ando T 2009 *Solid State Comm.* **27** 1123
[22] Koshino M and McCann E 2009 *Phys. Rev.* B **80** 165409
[23] Koshino M 2010 *Phys. Rev.* B **81** 125304
[24] Perdew J P and Zunger A 1981 *Phys. Rev.* B **23** 5048
[25] Gonze X, Stumpf R and Scheffler M 1991 *Phys. Rev.* B **44** 8503
[26] Kleinman L and Bylander D M 1982 *Phys. Rev. Lett.* **48** 1425
[27] Monkhorst H J and Pack J D 1976 *Phys. Rev.* B **13** 5189
[28] Srivastava G P 1999 *Theoretical Modelling of Semiconductor Surfaces* (Singapore:World Scientific)
[29] Srivastava G P 1993 *J. Phys. Condens. Matter* **5** 4695
[30] Grimme S 2006 *J. Comput. Chem.* **27** 1787
[31] Tkatchenko A and Scheffler M 2009 *Phys. Rev. Lett.* **102** 073005
[32] Ruiz V G, Liu W, Zojer E, Scheffler M and Tkatchenko A 2012 *Phys. Rev. Lett.* **108** 146103
[33] Dion M, Rydberg H, Schröder E, Langreth D C and Lundqvist B I 2004 *Phys. Rev. Lett.* **92** 246401
[34] Lee K, Murray E D, Kong L, Lundqvist B I and Langreth D C 2010 *Phys. Rev.* B **82** 081101
[35] Brako R, Sokcevic D, Lazic P and Atodiresei N 2010 *New J. Phys.* **12** 113016
[36] Vanin M, Mortensen J J, Kelkkanen A K, Garcia-Lastra J M, Thygesen K S and Jacobsen K W 2010 *Phys. Rev.* B. **81** 081408
[37] Zacharia R, Ulbricht H and Hertel T 2004 *Phys. Rev.* B **69** 155406